

## Morphodynamic modeling the impact of large-scale embankment on the large bar in a convergent estuary

Xie, Dongfeng; Wang, Zheng Bing ; van der Wegen, Mick; Huang, Junbao

**DOI**

[10.1016/j.margeo.2021.106638](https://doi.org/10.1016/j.margeo.2021.106638)

**Publication date**

2021

**Document Version**

Accepted author manuscript

**Published in**

Marine Geology

**Citation (APA)**

Xie, D., Wang, Z. B., van der Wegen, M., & Huang, J. (2021). Morphodynamic modeling the impact of large-scale embankment on the large bar in a convergent estuary. *Marine Geology*, 442, Article 106638. <https://doi.org/10.1016/j.margeo.2021.106638>

**Important note**

To cite this publication, please use the final published version (if applicable). Please check the document version above.

**Copyright**

Other than for strictly personal use, it is not permitted to download, forward or distribute the text or part of it, without the consent of the author(s) and/or copyright holder(s), unless the work is under an open content license such as Creative Commons.

**Takedown policy**

Please contact us and provide details if you believe this document breaches copyrights. We will remove access to the work immediately and investigate your claim.

1 **Morphodynamic modeling the impact of large-scale embankment on the large**  
2 **bar in a convergent estuary**

3 **Dongfeng Xie<sup>a</sup>, Zheng Bing Wang<sup>b,c</sup>, Mick Van der Wegen<sup>c,d</sup>, Junbao Huang<sup>a</sup>**

4 <sup>a</sup>Zhejiang Institute of Hydraulics and Estuary, Hangzhou, China; Zhejiang Provincial Key  
5 Laboratory for Estuarine and Coastal Research, China

6 <sup>b</sup>Faculty of Civil Engineering and Geosciences, Delft University of Technology, The Netherlands

7 <sup>c</sup>Deltares, P.O. Box 177, 2600 MH Delft, The Netherlands

8 <sup>d</sup>IHE Delft, PO Box 3015, 2601 DA Delft, the Netherlands

9 Corresponding author: Dongfeng Xie ([dongfeng.xie@hotmail.com](mailto:dongfeng.xie@hotmail.com)).

10

11 **Abstract:** Many alluvial estuaries worldwide include an inside bar system, a large sediment  
12 deposit deeply stretched into the estuary. A good example of such a system is the large sediment  
13 deposit in the Qiantang Estuary, China. Its length and height reach 130 km and 10 m, respectively.  
14 Bathymetrical comparison reveals that the large bar has moved seaward by around 15 km over the  
15 last decades, probably related to the large-scale coastal embankment project. This motivated a  
16 quantitative investigation of the impact of estuarine planform on the inside bar development. The  
17 bar morphology is reproduced by means of an idealized 1-D morphodynamic model. Model results  
18 suggest that the bar movement is related to a decreasing tidal prism, increasing flood dominance  
19 in the lower reach and enhanced ebb currents in the upper reach, in response to the embankment.  
20 The timescale of the morphological response is only several years. The rapid response is related to  
21 the strong tidal currents and large sediment fluxes within the estuary. Sensitivity experiments show

22 that the location and dimensions of the bar are related to the convergence length of the estuary. A  
23 decrease of the convergence length causes seaward movement and shortening and lowering of the  
24 bar. The bar dimensions also depend on the ratio between river and tidal discharges. When the ratio  
25 increases, the bar apex moves seaward and the elevation decreases. The bar movement has  
26 significantly influenced the tidal bore in the Qiantang Estuary.

27 **Keywords:** morphodynamic modeling; inside bar dimensions; coastal embankment; tidal bore;  
28 Qiantang Estuary; coastal management

29

## 30 **1. Introduction**

31 Located at the transitional zone between river and the sea, estuaries are of enormous societal  
32 and environmental importance. They provide accessibility for navigation, freshwater and fertile  
33 soil of the adjacent floodplains. Therefore most densely populated areas of the world are situated  
34 near estuaries. Estuaries also play an important role in global carbon/biogeochemical cycling, and  
35 serve as a crucial feeding and breeding ground for various flora and fauna (e.g., [Dyer, 1997](#);  
36 [Townend et al., 2012](#); [Savenije, 2012](#)). The estuarine morphology is shaped by natural forcing such  
37 as river flow, tides, waves and human activities such as land reclamation, navigational training,  
38 sand mining and dam construction. Particularly in the last two centuries, anthropogenic impact has  
39 increased and has, in many cases, overwhelmed the influences of natural developments, causing  
40 many estuaries and deltas to be in a state of rapid transition ([Wang et al., 2015](#); [Hoitink et al.,](#)  
41 [2017](#)). From the perspective of sustainable coastal management, it is of major significances to  
42 understand and predict the morphodynamic behavior of estuaries in response to changing natural

43 conditions and human activities.

44 In estuarine environments, the seaward decreasing river flow impact is coupled with the  
45 landward decreasing impact of tidal motion. There exists a certain place where seaward sediment  
46 transport by river offsets landward sediment transport by tides (Dalrymple and Choi, 2007; Choi  
47 et al., 2020). This inevitably results in the development of sediment bodies, like distributary mouth  
48 bars, river-channel bars and tidal ridges. They build up the skeleton of estuaries and play a major  
49 role in the hydrodynamics and sediment transport (Zhang X et al., 2020).

50 Morphodynamic models provide a powerful tool to investigate the formation and underlying  
51 physical mechanisms of observed morphological patterns in the real world. Geleynse et al. (2011);  
52 Leonardi et al., 2013; Xie et al. (2017a); Hoitink et al. (2017) and Luan et al. (2018) are examples  
53 of recent research efforts to address mouth bar formation, and its morphodynamic response to  
54 riverine sediment supply. Van der Wegen and Roelvink (2012), Dam et al. (2016) and Nnafie et al.  
55 (2018, 2019) addressed the importance of the estuarine planform and historic land reclamation  
56 works on the evolution of the channel-shoal patterns. However, the morphodynamics of an  
57 extended inside bar, a first order morphological feature located in the inner estuary, remains  
58 relatively unexplored, especially considering their response to human activities such as land  
59 reclamations.

60 The Qiantang Estuary is one of the largest macro-tidal estuaries worldwide (Fig. 1). A large  
61 longitudinal bar is developed in the inner estuary. It is the largest estuarine sediment deposit in  
62 China. With a length of around 130 km, and the highest part about 10 m above the estuary's bed,  
63 its spatial scale is at least one order larger than single or complex sandbars observed in many other

64 estuaries. The formation of this bar is due to the ample sediment supply from the adjacent  
65 Changjiang (Yangtze) Estuary, of which the fluvial sediment load used to be 450 million tons per  
66 year, and is transported along shore and into the Qiantang Estuary (Milliman et al., 1985; Chen et  
67 al., 1990; Zhang et al., 2014, 2015). In recent years, several morphodynamic models have been  
68 employed to reproduce the formation of the large bar and explore the underlying physical  
69 mechanisms (Yu et al., 2012; Xie et al., 2017b; Hu et al., 2018). Based on a long series of  
70 bathymetric data in the estuary, Xie et al. (2018) suggested that under natural conditions, the  
71 morphodynamics of the Qiantang Estuary is controlled by a combination of river flow and tides,  
72 especially by river flood events and tidal bores.

73 Since the 1960s, a large-scale coastal embankment project (LCEP) narrowing the Qiantang  
74 Estuary has been gradually implemented (Fig. 1). The planform of the estuary has been changed  
75 considerably. Several studies have focused on the influences of the LCEP on the hydrographical  
76 regime, using water level records or numerical modeling based on shoreline changes (Zou and  
77 Shen, 2017; Jin et al., 2020). But still there exist a gap between the hydrographic change and  
78 morphological evolutions. Recent analysis of the bathymetrical data revealed that the bar has  
79 shown a seaward movement in the last decades (Fig. 2). This raises scientific questions on the  
80 underlying physical processes for the bar movement and to what extent the estuarine planform can  
81 determine the dimensions of the bar within the estuary?

82 The large bar of the Qiantang Estuary is also the region where one of the most spectacular  
83 and fascinating tidal bore in the world occurs, a particular hydraulic phenomenon readily observed  
84 as a near-vertical wall of water traveling upriver during flood tide (Bartsch-Winkler and Lynch,

85 [1988; Chanson, 2012](#)). It has been long recognized that the large bar is one of the prerequisites for  
86 the bore formation ([Chen et al., 1964; Chen et al., 1990; Han et al., 2003](#)). The drastic landward  
87 rising bed level in the bar reach reduces the water depth and promotes the tidal wave deformation  
88 and eventually breaking. In recent years, several studies have focused on the turbulence properties  
89 and associated sediment transport of tidal bore based on short-term (e.g., a spring-neap tidal cycle)  
90 field observations and numerical models (e.g., [Pan and Huang, 2010; Fan et al., 2014; Tu et al.,](#)  
91 [2021](#)). However, few focused on the impact of anthropogenic morphological changes on the bore  
92 propagation.

93 In this contribution, we aim to explore the influence of estuarine planform on the  
94 morphological development of an inside bar, taking the large bar in the Qiantang Estuary as an  
95 example. Specific objectives are: (1) to reproduce the morphological response of the inside bar in  
96 the Qiantang Estuary to the large-scale coastal embankment works and analyze the underlying  
97 physical mechanisms; (2) to determine the controls of the bar dimensions and location and to  
98 develop a comprehensive framework of the bar morphodynamics; (3) to explore the influence of  
99 the bar evolution on the tidal bore characteristics. The Qiantang Estuary is surrounded by one of  
100 the most developed regions in China. Due to its large extent, the morphodynamic evolution of the  
101 inside bar affects the entire environment of the estuary. Therefore, studying the morphodynamic  
102 evolution of the large bar in the Qiantang Estuary not only improves our understanding of the  
103 morphodynamic behavior of the inside bar but also helps the coastal development and marine  
104 spatial planning of local government.

## 105 **2. Study area**

106 The Qiantang Estuary is a macro-tidal convergent estuary, located immediately south of the  
107 Changjiang (Yangtze) Estuary (Fig.1). The length is 282 km and the width narrows from 98.5 km  
108 at the mouth to less than 1 km at the landward end. The estuary can be divided into three reaches  
109 (Han et al., 2003). The riverine reach, extending over 87 km upstream Zhakou to the Fuchun Power  
110 Station, is dominated by river discharge while the effects of tides are limited. It is mainly composed  
111 of coarse sand and gravel and the bed is relatively stable. The seaward reach downstream Ganpu,  
112 also well known as the Hangzhou Bay, is 87 km long and controlled by tidal currents. With the  
113 sediment input from the Changjiang Estuary, the Hangzhou Bay has continuously experienced net  
114 deposition, with an average accumulation rate of 1.15 cm over the recent 100 years (Dai et al.,  
115 2014). The estuarine reach between Zhakou and Ganpu, with a length of 108 km, is floored by  
116 easily erodible, well-sorted silt and clay floored on the bed. It is controlled by the combination of  
117 river flow and tidal currents. The morphological evolution in this reach is comparatively dynamic.

118 The most remarkable morphological feature of the estuary is the large longitudinal bar (Figs.  
119 1b and 2). It starts from Zhapu at the middle Hangzhou Bay and elongates by about 130 km  
120 landward. The bed level rises gradually from about -10 m at Zhapu to 1 m at the Qibao - Cangqian  
121 reach, and then gradually decreases to be about -20 m (with respect to the Chinese National Vertical  
122 Datum of 1985, the same below). There are several bends upstream of Ganpu. The thalweg and  
123 tidal flats are developed at the concave and the convex banks, respectively (Fig. 1b). Between  
124 Zhapu and Jinshan, a large tidal channel and a tidal flat have developed in the northern and  
125 southern Hangzhou Bay, respectively (Han et al., 2003; Xie et al., 2009, 2017b). Downstream from  
126 Jinshan, there is a large subaqueous plain with an average depth of about 11 m.

127 The annual discharge from the Qiantang River is 952 m<sup>3</sup>/s, much smaller than the tidal prism  
128 at the mouth that can be 30×10<sup>9</sup> m<sup>3</sup> (tidal flow discharge in the order of 10<sup>6</sup> m<sup>3</sup>/s) during spring  
129 tides (Xie et al., 2017a). Due to the monsoon climate, river discharge is characterized by seasonal  
130 and interannual variations. The period between April and July is the wet season, with an average  
131 peak value of 1893 m<sup>3</sup>/s in June while the period between August and next March is the dry season,  
132 with a monthly discharge varying between 438 and 592 m<sup>3</sup>/s (Xie et al., 2017b). Over the years,  
133 the annually averaged discharge fluctuates between 319 and 1390 m<sup>3</sup>/s. During high flow season,  
134 the flood peaks can be more than 10,000 m<sup>3</sup>/s, with the daily maximum being 12,787 m<sup>3</sup>/s since  
135 the 1960s (Han et al., 2003). The Qiantang Estuary is strongly influenced by the river flood events  
136 and the tidal bore in the estuary, one of the largest in the world (Bartsch-Winkler and Lynch, 1988;  
137 Pan and Huang, 2010). As a result, the estuary is characterized by active morphological changes  
138 on seasonal and interannual time scales. Especially in the inner estuary the local bed level change  
139 can be more than 5 m in several months (Chien et al., 1964; Han et al., 2003; Xie et al., 2018) .

140 The tides in the estuary originate from the East China Sea and are mainly composed of a  
141 semidiurnal M<sub>2</sub> constituent. The mean tidal range is about 3.2 m at the mouth (Xie et al., 2017a).  
142 Landward width convergence and shallower bathymetry considerably deform the tidal waves  
143 upstream evolving into the world famous Qiantang bore. The tidal range increases landward and  
144 reaches its maximum at Ganpu, with a multi-year average of 6.0 m, and then decreases landward  
145 due to bed friction. Wind waves are weak in this area, with an annually averaged wave height of  
146 0.5 m at the Tanxu station (water depth of about 10 m) in the Hangzhou Bay (Han et al., 2003).

147 Due to the large width to depth ratio, the main channel of the Qiantang Estuary used to

148 meander continuously, and the coastal protection revetments used to collapse frequently, resulting  
149 in lack of resources for development and navigation channel maintenance. Since the 1960s, a large-  
150 scale coastal embankment project has been carried out for the purpose of flood defense and land  
151 reclamation amongst others (Li and Dai, 1986; Han et al., 2003). The LCEP was implemented  
152 gradually seaward and basically finished in the 2010s (Fig. 2). The land reclamation mainly  
153 occurred at the middle and high flats. So far, more than 1000 km<sup>2</sup> land has been reclaimed and the  
154 planar shape of the estuary has been largely changed. For example, the width at Yanguan has  
155 decreased from about 10 km to about 2.5 km and at Ganpu from about 22 km to 18 km.

156

### 157 **3. Model description**

#### 158 **3.1. Model setup**

159 The inside bar in the Qiantang Estuary is a longitudinal morphological feature, with the length  
160 much larger than the width and depth. Since the main body of the inside bar is located in the  
161 estuarine reach where the width is relatively small, the lateral variation of the morphology is less  
162 important. Therefore, a 1-D model can fulfill the controlling processes of the hydrodynamics and  
163 morphological evolution. Compared to the complex morphodynamic models that contain the state-  
164 of-the-art physical descriptions and parameterizations, an idealized model focuses on the  
165 prevailing morphological processes and favors an examination of the underlying physical  
166 mechanisms in a straightforward manner, through input reductions including simplified geometry  
167 and boundary conditions and formulations.

168 We construct an idealized 1-D morphodynamic model based on the Delft3D software

169 (Deltares, 2016), which has been widely used for hydrodynamics and morphodynamics in  
170 estuarine environments (e.g., Wang et al., 1995; Hibma et al., 2004; Van der Wegen and Roelvink,  
171 2008; Van der Wegen and Jaffe, 2014; Guo et al., 2014; Zhou et al., 2017; Nnafie et al., 2019).  
172 Flow is calculated based on the horizontal shallow water equations. Transport of the suspended  
173 sediment is based on the advection-diffusion equation, in which the erosion and deposition fluxes  
174 between the bed and the water column are calculated by the well-known Krone-Partheniades  
175 formulation (Partheniades, 1965). Bed elevation is dynamically updated at each computational  
176 time step, based on the conservation of sediment mass and multiplied by a morphological factor  
177 of 10 to enhance bed level change.

178 This study focuses on the influences of changes in estuarine planform on the morphodynamic  
179 development of the large bar and associated hydrographic regime. Two basic cases are set. The  
180 model domain mimics the outlines of the Qiantang Estuary in the 1950s and the 2010s,  
181 representing the estuarine planforms before and after the LCEP, respectively (Fig. 3). The domain  
182 consists of a 280 km long basin with a constant width of 1 km for the first 90 km followed by a  
183 width expanding to 100 km at the mouth. Compared to the 1950s case, the coastline in the 2010s  
184 case is narrowed by 8 km at 140 km and 4 km at 200 km (the x-coordinate is defined from the  
185 landward end, as shown in Fig. 3a). The initial bed level decreases linearly from 0 m at the  
186 landward end to -9 m at the seaward end, indicating a preliminary longitudinal bed slope of  $3.2 \times 10^{-5}$ .  
187

188 At the seaward boundary, the model is forced by a semidiurnal  $M_2$  tide with a tidal amplitude  
189 of 2 m. A suspended sediment concentration (SSC) of  $1.0 \text{ kg/m}^3$  is prescribed, close to the annual

190 average SSC at the mouth (ECCHE et al., 1992; Xie et al., 2017a). At the landward boundary,  
191 episodic river flood events are neglected so that we can focus on the long-term morphologic  
192 development of the large bar under human activities. A constant river discharge of 1000 m<sup>3</sup>/s is  
193 prescribed, close to the annually averaged discharge from the Qiantang River. The SSC is set to be  
194 0.15 kg/m<sup>3</sup>, denoting that the annual sediment supply from the Qiantang River is about 5×10<sup>6</sup> ton  
195 (Chen et al., 2006). Both the two cases are run for 3 years of morphodynamic evolution in which  
196 the bar system is formed. As a first approximation, we neglect the role of salinity stratification.

197

### 198 3.2. Model runs for sensitivity analysis

199 In order to obtain a more general understanding of the controls of the planform of the estuary  
200 on the bar dimensions, an additional group of numerical experiments is conducted (Table 1). The  
201 formulation of estuary convergence with a width reducing exponentially in landward direction has  
202 been well adopted in many studies and can be expressed by the following classical relation (e.g.,  
203 Friedrichs and Aubrey, 1994; Lanzoni and Seminara, 1998; Savenije, 2012):

$$204 \quad B = B_0 \exp\left(-\frac{L-x}{L_b}\right) \quad (1)$$

205 in which  $B_0$  is the width at the mouth,  $L$  is the estuary length and  $L_b$  is the convergence length.

206 Based on the widths along the estuary in the 1950s and 2010s (upper right panel in Fig.1a), it can  
207 be found that the convergence length of the estuary has decreased from 65 km to 50 km, indicating  
208 an increase of the convergence. The width at the estuary mouth is fixed at 100 km, since it is  
209 determined by the geological background such as the Zhoushan archipelago. The width along the  
210 estuary is decreased exponentially landward with convergence lengths of 20, 40, 60, 80, 100 km,

211 respectively. The other model inputs are kept invariant.

212 In an alluvial estuary, river discharge and the associated sediment supply may play an  
213 important role, especially in the upper reach where smaller channel cross-sections and tidal prisms  
214 prevail. River flows attenuate tidal currents through enhanced tidal friction, and constrain landward  
215 saltwater intrusion by enlarging ebb currents (Godin, 1985; Savenije, 2012; Hoitink and Jay, 2016).  
216 As a result, considerable morphological changes in estuarine environments may take place due to  
217 the variations of river discharges. In terms of the Qiantang Estuary, it has been recognized that  
218 during the high flow periods, the river flow erodes the bed and transports sediment seaward  
219 whereas during the low flow periods, the tidal currents transport sediment landwards leading to  
220 deposition in the inner estuary (Han et al., 2003; Xie et al., 2017b; Xie et al., 2018). In this study,  
221 in order to explore the controls of river discharge on the bar dimensions, a series of sensitivity runs  
222 are added on the basis of the two basic cases, with the river discharge varying from 250 to 2000  
223  $\text{m}^3/\text{s}$  with an interval of 250  $\text{m}^3/\text{s}$ . These values fall in the reasonable range of the river discharges  
224 of the Qiantang River, as mentioned in the previous section.

225

## 226 **4. Model results**

### 227 **4.1. Morphological evolution**

228 Figure 4 illustrates the processes of the morphological evolution of the estuary in the 1950s  
229 and 2010s cases. In the model the large bar is formed in 3 years, in agreement with recent studies  
230 (Xie et al., 2017b; Hu et al., 2018). In the 1950s case, the reach upstream 50 km has significantly  
231 eroded. The sediment is transported seaward. The cumulative sediment transport through the 50

232 km transect over 3 years is  $5.7 \times 10^6 \text{ m}^3$ . The reach downstream 175 km is eroded, tending to evolve  
233 toward a subaqueous plain, and the sediment is transported landward. The cumulative sediment  
234 transport through the 175 km transect over 3 years is  $57.5 \times 10^6 \text{ m}^3$ . As a result, sediment of  
235  $63.2 \times 10^6 \text{ m}^3$  is accumulated between 50 and 175 km, and a large bar is gradually developed. More  
236 than 90% of the sediment accumulated in the bar region is from seaside, consistent with previous  
237 studies on the sediment sources of the large bar (Chen et al., 1990; Zhang et al., 2015). The bar  
238 apex is located at 103.5 km and its elevation is 1.10 m. Morphological development in the 2010s  
239 case is similar. The bar apex is located at 122.4 km and its elevation is 0.54 m. The cumulative  
240 sediment accumulation at the bar area is  $58.0 \times 10^6 \text{ m}^3$ , smaller by  $5.2 \times 10^6 \text{ m}^3$  than that in the 1950s  
241 case. Compared to the 1950s case, the bar apex in the 2010s case has moved seaward by 16 km  
242 and lowered by 0.86 m. The landward slope of the bar (upstream the apex) is eroded by 1.5 m on  
243 average whereas the seaward slope (downstream the apex) is accumulated by 1.0 m on average.

244 Overall, the simulated longitudinal profiles after 3 years are comparable with the real  
245 situations (Fig. 3), indicating that the model can skillfully reproduce the morphological response  
246 of the bar to the LCEP. Furthermore, the longitudinal length of the bar has decreased from 137.3  
247 km to 128.8 km. This is mainly related to the seaward movement of the landward slope of the bar,  
248 because the location of tail of the bar has hardly changed.

249 Similar to the 2-D morphodynamic modeling of Xie et al. (2017b), a longer than 3 year  
250 simulation shows that the bar grows continuously to an unrealistic height ( $\gg 10 \text{ m}$ ). In reality, the  
251 growth will be constrained by erosion during high river discharge periods, i.e. river flood events.  
252 In the Qiantang Estuary, flood events occur almost in each year (Han et al., 2003). Flood events

253 erode seriously the bed in the inner estuary and export sediment seaward. Over a long enough time  
254 span, the sediment input by tides can be balanced by sediment export by flood events (Xie et al.,  
255 2017b; Xie et al., 2018).

256

## 257 4.2. Hydrodynamic and sediment transport changes

258 The hydrodynamics and associated sediment transport are responsible for the morphological  
259 dynamics in estuaries. Exploring the origin of the large bar in the Qiantang Estuary (Yu et al., 2012;  
260 Xie et al., 2017b; Hu et al., 2018) suggested that landward sediment transport by flood dominance  
261 is the main cause for the bar formation. Here we focus on the change of the hydrodynamic regime  
262 induced by the change of the estuarine planform.

263 In the initial state, both the high and low water levels increase landward due to backwater  
264 effects (e.g., Savenije, 2012; Hoitink and Jay, 2016) (Fig. 5a). The tidal range maintains around 4  
265 m downstream of 90 km and decreases gradually landward due to the bed friction. The tidal bore  
266 is also reproduced (Fig. 5b). After the coastal embankment, the high water level increases upstream  
267 150 km due to the enhanced reflection of the tidal wave. The maximum increase is about 0.5 m.  
268 The low water level increases upstream 100 km but decreases between 100 and 220 km.  
269 Subsequently, the tidal range upstream 200 km is increased, with the maximum being 0.6 m.

270 Both flood and ebb velocities increase between 50 and 250 km, because the narrowing of the  
271 estuary converge the tidal energy. The maximum increase of the velocities appears at around 100  
272 km (Fig. 5c). Between 50 and 250 km, the flood maximum ( $u_f$ ) is larger than ebb maximum ( $u_e$ ),  
273 with a maximum ratio of  $u_f/u_e$  of 1.74, indicating the flood dominance (Fig. 5d). Downstream 50

274 km and upstream 250 km, the flood maximum is less than ebb maximum, indicating the ebb  
 275 dominance. After the coastal embankment, the flood dominance decreases upstream 90 km and  
 276 increases downstream 90 km. Overall, the changes of the flood and ebb velocities induced by the  
 277 embankment works are qualitatively consistent with the results of [Zou and Shen \(2017\)](#) who  
 278 simulated the influences of the LCEP on the hydrodynamics in the estuary using real coastline and  
 279 bathymetry.

280 The tidal prism  $Q_t$ , the ratio  $R$  between the river discharge and the tidal prism along the estuary  
 281 are calculated as follows:

$$282 \quad Q_t = \int_{t_0}^{t_0+T_f} UHBdt \quad (2)$$

$$283 \quad R = \frac{\int_{t_0}^{t_0+T_f} qdt}{Q_t} \quad (3)$$

284 where  $U$  is the depth-averaged current velocity (m/s),  $H$  is the water depth (m),  $B$  is the width (m),  
 285  $t_0$  is the begin of flood period,  $T_f$  is the flood duration (s),  $q$  is river discharge ( $\text{m}^3/\text{s}$ ). The sediment  
 286 fluxes of flood and ebb tides are function of the tidal prism, SSC and river discharge.

287 The tidal prism at the estuary mouth is about  $28 \times 10^9 \text{ m}^3$  and decreases gradually landward  
 288 (Fig. 5e), in agreement with the field observation ([Xie et al., 2017a](#)). Correspondingly, the ratio  $R$   
 289 decreases from 0.18 at the landward end to less than 0.001 at the seaward end. After the  
 290 embankment, the tidal prism decreased by about 30%. Hence the ratio  $R$  is increased accordingly  
 291 (Fig. 5f). Sediment flux at the mouth is about  $2.2 \times 10^6 \text{ m}^3$  and increases slightly landward but then  
 292 decreases (Fig. 5g). The net sediment flux is in the order of  $10^4 \text{ m}^3$  per tidal cycle, being negative  
 293 between 90 and 200 km, and positive upstream 90 km and downstream 250 km (Fig. 5h). Since

294 the bed level change is related to the spatial gradient of sediment transport rate, sediment will  
295 accumulate in the bar area. After the embankment, the changes of sediment fluxes are similar to  
296 those of tidal prisms. The sediment flux downstream 150 km decreases by about 20%. The net  
297 sediment transport decreases between 100 and 170 km whereas increases between 170 and 250  
298 km.

299 In the region of bar formation, both the high and low water levels upstream 100 km is lowered  
300 due to the bed erosion in the upper reach (compare Fig.5a and Fig. 6a). The longitudinal water  
301 level slope is decreased accordingly. The difference between the high levels in the two cases is  
302 comparable with that at the initial stage, indicating that the influence of the bathymetrical change  
303 is limited and the change of the high level is mainly related to the embankment. The low water  
304 level in the 2010s case is about 0.1 m lower than in the 1950s case, consistent with the recent  
305 finding based on field data by [Jin et al. \(2020\)](#) who found that the annual low levels at Zhakou,  
306 Qibao and Yanguan stations have shown decreasing trends since 1960s, with the magnitude  
307 between 0.05 and 0.2 m. This is because the low level in the upper reach is mainly related to the  
308 local bed levels ([Han et al., 2003](#)). The bed erosion of the upper reach in the 2010s case is more  
309 apparent than in the 1950s case (Fig. 4). The low level in the bar region is apparently influenced  
310 by the bathymetry, and a fast lowering of the low level occurs from 100 km to 160 km. The low  
311 level between 100 and 160 km is 0.1-0.4 m higher in the 2010s case than in the 1950s case, due to  
312 the accumulation in the downstream slope of the large bar. As a result, the tidal range in the inner  
313 estuary increases by about 0.4 m (Fig. 6b) , consistent with field data ([Pan and Han, 2017](#)). Such  
314 a tidal amplification is similar to the sand extraction in the Pearl Estuary, Southern China and and

315 channel deepening in the Ems Estuary (Zhang et al., 2010; van Maren et al., 2015; Dijkstra et al.,  
316 2019). However, the tidal amplification in the Qiantang Estuary is not directly induced by human  
317 activities but indirectly by the response of the morphodynamic system to the LCEP.

318 In both cases, the ebb maximum in the inner estuary decrease due to the bed erosion (Fig. 6c).  
319 Compared to the velocities in the 1950s case, both the flood and ebb maximum increase between  
320 50 and 130 km. Subsequently, the ratio  $u_f/u_e$  increase upstream 100 km, consistent with the tidal  
321 amplification. The peak of  $u_f/u_e$  still appears in the bar area, but its location moves seaward by 18  
322 km (Fig. 6d).

323

#### 324 **4.3. Influence of river discharge**

325 Fig. 7 shows an example of the longitudinal profiles of the estuary in the basic cases under  
326 the variation of river discharge, and the corresponding bed level changes under the low ( $500 \text{ m}^3/\text{s}$ )  
327 and high ( $1500 \text{ m}^3/\text{s}$ ) discharges, compared with that under the intermediate flow ( $1000 \text{ m}^3/\text{s}$ ). In  
328 the low flow cases, sediment accumulation and erosion occur in the upper and lower parts of the  
329 bar, respectively, and subsequently the bar moves landwards. Vice versa in the high flow cases.  
330 The magnitudes of bed level change in the high flow case is smaller than in the low flow case,  
331 implying the bed level change is more sensitive to the river discharge variation in the low flow  
332 period.

333 Compared to the 1950s case, the region with significant bed level changes in the 2010s case  
334 moves seaward by about 10 km. For example, in the 1950s case, the transitional point between  
335 erosion and accumulation is located at 124 km and 132 km under the discharge of  $500 \text{ m}^3/\text{s}$  and

336 1500 m<sup>3</sup>/s, respectively; whereas in the 2010s case it is at 132 km and 140 km, respectively (Fig.  
337 7b). [Chen et al. \(1990\)](#); [Han et al. \(2003\)](#) suggested continuous water and sediment exchange  
338 between the estuary and the Hangzhou Bay. Our model results suggest that this exchange has  
339 changed as a result of the LCEP and the seaward movement of the large bar.

340 The location and elevation of the bar apex correlates well with the river discharge (Fig. 8).  
341 With the river discharge increasing from 250 m<sup>3</sup>/s to 2000 m<sup>3</sup>/s, the bar apex in the 1950s case  
342 moves seaward from 89.3 km to 109.1 km and its elevation is lowered from 2.81 m to -0.66 m.  
343 [Chen et al. \(1990\)](#) found similar correlations by using bathymetrical and discharge data before the  
344 beginning of the LCEP. These correlations suggest the existence of a dynamic equilibrium for the  
345 large bar, with seasonal and interannual variations depending on river discharge variations, but in  
346 balance over longer time scales. This dynamic equilibrium was also found by [Fan et al. \(2016\)](#)  
347 based on time-series of satellite images of the seasonal and multi-year variations of channel  
348 morphology. With the implementation of the LCEP, the correlations have been changed. On  
349 average, the location of the bar apex in the 1950s and 2010s cases is at 101.4 km and 117.0 km,  
350 respectively, and the elevation of the bar apex is 0.80 m and 0.49 m, respectively.

351

#### 352 **4.4. Influence of estuary convergence**

353 Tidal prism depends on the estuarine planform to a large extent. One of the most important  
354 consequences of land reclamation is the reduction of tidal prism (e.g., [Friedrichs and Aubrey, 1994](#);  
355 [Lanzoni and Seminara, 1998](#); [Todeschini et al., 2008](#); [Pye and Blott, 2014](#); [Wang et al., 2015](#)). Fig.  
356 9a shows that the tidal prism at the estuary mouth correlates with the convergence length of the

357 estuary. With the  $L_b$  decreasing from 100 km to 20 km, the prism decreases from  $27.4 \times 10^9 \text{ m}^3$  to  
358  $12.1 \times 10^9 \text{ m}^3$ . Accordingly, the ratio  $R$  increases (Fig. 9b). The maximum ratio for the cases of 20,  
359 40, 60, 80 and 100 km are 2.8, 1.87, 1.40, 0.81 and 0.51, respectively. The ratio shows a rapid  
360 reduction seaward in the upper reach (0 - 50 km) and then a relatively gentle reduction in the lower  
361 reach.

362 Fig. 10 illustrates the bathymetries of the estuary under various convergence lengths. In all  
363 cases, the large bar evolves. With a decreasing convergence length, the bar moves seaward and  
364 becomes lower, consistent with the basic cases (Fig. 4). The apex location moves from 191.8 km  
365 to 60.4 km, and elevation of the apex decreases from 3.2 m to -6.7 m, if the convergence length  
366 decreases from 100 km to 20 km. Moreover, the bar length decreases from 117.2 km to 4.6 km.  
367 Clear power or logarithmic relationships exist between the bar location as well as dimensions  
368 (elevation of the bar apex and the bar length) and the convergence length (Fig.11).

369 The formation of a tidal bore is related to the tidal range at the mouth, the funnel shape of the  
370 estuary which constraints the incoming tide and converges the tidal energy, and the subaqueous  
371 bathymetry which promotes the deformation of tidal wave (Lin, 2008; Dolgoplova, 2013;  
372 Bonneton et al., 2015). The strength of the tidal bore can be quantified using the relative Froude  
373 number  $F_r$  (Peregrine, 1966; Chanson, 2011):

374 
$$F_r = \frac{c - u_1}{\sqrt{gh_1}} \quad (4)$$

375 where  $c$  is the propagation speed of the bore,  $u_1$  and  $h_1$  are the current velocity and water depth  
376 prior to the arrival of the bore, respectively, and  $g$  is the gravitational acceleration. For  $F_r > 1.5 \sim 1.7$

377 the bore is breaking, while for  $1.3 < F_r < 1.5 \sim 1.7$  the bore is undular with limited breaking. By  
378 incorporating the analytical formula for the propagation speed of a bore (Pan et al., 2008) and  
379 formula (4), Zhang S et al. (2020) suggested the relative  $F_r$  can be calculated based on the local  
380 tidal range  $\Delta h$  and the current velocity prior to the bore  $h_u$ :

$$381 \quad F_r = \sqrt{\frac{1}{2} \left( \frac{\Delta h}{h_u} + 1.5 \right)^2 - \frac{1}{8}} \quad (4)$$

382 Fig. 12 shows the relative Froude number along the estuary after the bar formation in the cases  
383 of varying convergence length. Overall, the reach where  $F_r$  is larger than 1.7 is consistent with the  
384 morphological bulge of the bar, suggesting the importance of the bar on the tidal bore development.  
385 Similar to the development of the bar in the cases of various convergence lengths, the “bore reach”  
386 also shows a seaward movement. This is consistent with the observations and would be discussed  
387 below. Furthermore, the peak of  $F_r$  decreases with the decrease of the convergence length. The  
388 peak is 2.18, 2.17, 2.03, 1.75 and 1.41, respectively for the 5 convergence cases in order. This  
389 indicates that the tidal bore tends to be weakened with a narrowing of the estuary. A breaking bore  
390 would disappear while only an undular bore is formed if  $L_b$  is less than 20 km.

391

## 392 **5. Discussion**

### 393 **5.1. What determines the inside bar location and dimensions?**

394 Estuarine morphology results from an intricate balance between fluvial and marine processes  
395 (Dyer, 1997; Dalrymple and Choi, 2007). The relative strength of tidal prism and river discharge  
396 is often used to be a metric for the first-order estimate of estuarine morphology. For example,

397 downstream channel widening can be quantified by the ratio of the tidal and fluvial discharges  
398 (Nienhuis et al., 2018). Using a morphodynamic model of an idealized short estuary, Bolla  
399 Pittaluga et al. (2015) showed that the estuarine channel-bed slope tends to increase with  
400 decreasing fluvial discharge. The physical mechanism for the formation of the large inside bar in  
401 the Qiantang Estuary is also related to the ratio between the river flow and tidal prism. The  
402 planform of an estuary is one of the most important parameters controlling hydrodynamic and  
403 morphodynamic processes. Channel convergence causes a distortion of the tidal wave, strongly  
404 affects the hydrodynamics and forces the sediments to move towards the inner part of the estuary  
405 (e.g., Friedrichs and Aubrey, 1994; Lanzoni and Seminara, 1998; Todeschini et al., 2008; Savenije,  
406 2012). Given the fact that the river discharge is invariable in the last decades, the river flow - tidal  
407 prism ratio  $R$  depends on the variation of the tidal prism. Especially the decrease of the  
408 convergence length induces a reduction of tidal prism at the estuary mouth and subsequently an  
409 increase of the ratio  $R$  (Fig. 5e and Fig. 10a). Hence the role of river discharge in the inner estuary  
410 is relatively increased, which can push the large bar seaward. Furthermore, sensitivity analysis by  
411 numerical experiments show that not only the bar location but also the bar elevation and bar length  
412 correlates well with the estuary convergence. On the other hand, when the planform of the estuary  
413 is fixed, the bar dimensions are influenced largely by the variations of the river discharge. The role  
414 of river discharge turns out to be more apparent in the case of stronger convergence of the estuary  
415 (Fig. 6 and 7).

416 Tidal asymmetry is an important indicator for the sediment transport and morphological  
417 pattern development (Wang et al., 2002; Van der Wegen and Roelvink, 2008; Guo et al., 2014;

418 [Zhou et al., 2018](#)). The middle reach of the estuary is characterized by flood dominance (Fig. 5d).  
419 With the narrowing of the estuary, such reach is moved seaward slightly, and the area of sediment  
420 accumulation moves seaward (Fig. 5h).

421 Model results in this study show that the seaward movement of the bar induced by the LCEP  
422 has led to significant accumulation of the seaward slope of the bar (Fig. 4). Actually the accelerated  
423 accumulation rate can extend to the inner Hangzhou Bay. Based on historical bathymetries in the  
424 Hangzhou Bay, [Xie et al. \(2017c\)](#) found the accumulation rate in the inner Hangzhou Bay (between  
425 Jinshan and Ganpu) has been apparently increased from 2.4 cm/a during the period of 1959 - 2003  
426 to 13.4 cm/a during the period of 2010 - 2014. The inner Hangzhou Bay can be seen as the tail of  
427 the large bar (Fig. 2). Hence the model results explain the physical mechanism of morphological  
428 development since the 1960s in the Qiantang Estuary as well as the inner Hangzhou Bay.

429 Besides the estuarine planform, sediment supply is another potential factor for the  
430 morphological development. The Qiantang Estuary is one of the sinks of the Changjiang River  
431 sediment ([Milliman et al., 1985](#); [Chen et al., 1990](#); [Zhang et al., 2014, 2015](#)). In recent years,  
432 sediment load of the Changjiang River has been decreasing sharply from more than  $4.5 \times 10^8$  t/a  
433 to less than  $1.5 \times 10^8$  t/a due to soil conservation and dam constructions in the Changjiang River  
434 basin, especially since the impoundment of the Three Gorges Dam in 2003 ([Gao and Wang, 2008](#);  
435 [Yang et al., 2011](#); [Milliman and Farnsworth, 2011](#); [Dai et al., 2016](#)). As a result, the Changjiang  
436 Estuary has shifted from a sediment sink to a sediment source ([Yang et al., 2011](#); [Dai et al., 2018](#);  
437 [Mei et al., 2018](#); [Dai et al., 2021](#)). Hydrological surveys by [Xie et al. \(2017a\)](#) revealed that the  
438 annually-averaged net sediment flux into the Hangzhou Bay mouth has decreased slightly by about  
439 10% after 2003. The slight decrease sediment supply at the bay mouth caused the erosion in the  
440 outer bay in recent years ([Dai et al., 2014](#); [Xie et al., 2017c](#)). However, its influence on the inner

441 bay and the Qiantang Estuary has been overwhelmed by the large-scale embankment project,  
442 because the erosion of the outer bay provides a sediment source for the inner bay (Xie et al., 2017c).  
443 It can be concluded that the morphological adjustment of the large sand bar in the Qiantang Estuary  
444 in the last decades is mainly related to the LRNP.

445

## 446 **5.2. The rapid response of the bar to the estuary narrowing**

447 Coastal embankment works can be carried out in a relatively short period, whereas the  
448 morphological response of the estuary is relatively slow (Wang et al., 2015). In most estuaries the  
449 timescale for the morphology to adapt to the new hydrodynamic conditions is usually in the order  
450 of decades to centuries (Van der Wegen and Roelvink, 2012; Nnafie et al., 2018). The narrowing  
451 project of the Qiantang Estuary started in the earlier 1960s and basically finished in the 2010s. The  
452 project was implemented gradually seaward by several stages as shown in Fig. 1a. The morphology  
453 of the estuary has been changed sequentially (Pan and Han, 2017). For a long-term  
454 morphodynamic modeling the initial bathymetry and the specific process of the narrowing may  
455 influence the formed morphological patterns to a certain extent (Van der Wegen and Roelvink,  
456 2008; Zhou et al., 2017; Nnafie et al., 2019). In this study, we excluded the actual process of the  
457 project implementation by using simplified planforms and the same initial bathymetry before and  
458 after the LCEP, in order to focus on the influences of estuarine planform and the first-order controls  
459 of the large bar.

460 It turned out that the timescale of morphological response in the Qiantang Estuary is only  
461 several years, one or two orders faster than most other estuaries (Xie et al., 2017b; Hu et al., 2018).

462 The timescale for the morphological evolution is related to the sediment transport rate (Van Rijn,  
463 1993). The Qiantang Estuary is characterized by the strong tidal currents, especially influenced by  
464 the tidal bore, which result in large sediment transport rate (Han et al., 2003; Pan and Huang, 2010;  
465 Fan et al., 2014; Xie et al., 2018). Field observations showed that sediment flux over a flood or  
466 ebb period at the Ganpu transect is in the order of  $10^6$  m<sup>3</sup> (Han et al., 2003) and during normal  
467 river discharge periods the sediment accumulation in the estuarine reach can be in the order of  $10^6$   
468 m<sup>3</sup> in several months (Xie et al., 2018), in agreement with the present model results.

469 To the authors' knowledge, the Sittaung Estuary, Myanmar, is the only macro-tidal estuary  
470 comparable with the Qiantang Estuary in terms of the fast morphodynamic adaptation rate. The  
471 length of the estuary is 220 km, and it is also funnel-shaped. Sediments are also constituted by silt  
472 and clay with median grain size ranging between 0.02 and 0.04 mm (Shimozono et al., 2019; Choi  
473 et al., 2020). Recently, Ahmed et al. (2019) reproduced the morphological patterns in the Sittaung  
474 Estuary using a morphodynamic model. Starting from an initial bed with a constant slope, the  
475 channel-shoal pattern in recent years was reproduced well with a calculation time of only several  
476 months.

477

### 478 **5.3. The influence of the bar evolution on the tidal bore**

479 The Qiantang Estuary is characterized by one of the biggest tidal bores in the world. The bore  
480 scenes attract millions of tourists each year. It is also an important cultural resource, symbolizing  
481 the local people's spirit of trendsetter. Therefore, to what extent the LCEP influences the Qiantang  
482 bore is one of great interests to coastal scientists, engineers and managers.

483 Historically, the location of the bore occurrence was further west than the present age. For  
484 example, in the Song Dynasty, about 1000 years ago, the location used to be upstream of Wenyan,  
485 about 70 km upstream of Yanguan ([Chen et al., 1964](#)). Presently the most spectacular tidal bore  
486 occurs at the Yanguan reach ([Lin, 2008](#); [Pan and Huang, 2010](#); [Tu et al., 2021](#)). In recent years, a  
487 breaking bore has been frequently witnessed at Shangyu, about 40 km downstream of Yanguan,  
488 indicating that the place of the bore occurrence has probably moved further seaward.

489 However, aside from the historical documents of the Qiantang bore, field records of the bore  
490 are very scarce, making it difficult to link the bore formation with the long-term morphological  
491 evolution. Based on scale model experiment, [Zeng et al. \(2017\)](#) suggested that embankments near  
492 Jianshan, about 10 km long and 2.5 km wide, resulted in an increase of about 0.1 m of the bore  
493 height, due to the enhancement of the tidal wave reflection. They also suggested that if a larger  
494 embankment is carried out, the tidal prism from the East China Sea will be decreased and hence  
495 weaken the Qiantang bore. Recently, based on numerical models, [Zhang S et al. \(2020\)](#) and [De  
496 Ridder \(2017\)](#) tested the influences of the bathymetrical changes on the tidal bores in the Qiantang  
497 Estuary and the Sittuang Estuary, respectively. Increasing or reducing the bed elevation in the  
498 estuaries by a uniform value, their results showed that the bathymetry plays an important role in  
499 the bore formation and propagation. In this study, we reproduced the morphological response of  
500 the bar to the LCEP and predicted the bar location and dimensions under further narrowing in the  
501 future. It turned out that with the change of the estuarine planform and the seaward movement of  
502 the large bar, the reach for breaking bore conditions moves seaward. This explains the physical  
503 mechanisms for the historical and recent evolutions of the place of the bore occurrence. It is notable

504 that if the estuary is narrowed further in the future, the place of the bore occurrence would move  
505 further seaward, and would be even in danger of disappearing (Fig. 12). For the estuarine  
506 regulation in the future, attention must be paid to the influence of the morphological evolution on  
507 the tidal bore

508 The tidal bore is highly influenced by the bar morphology. In turn, the tidal bore also exerts  
509 great impact on the bar morphology because of the associated strong currents and sediment  
510 transport capacity. The results of the present morphodynamic model show that in addition to the  
511 seaward movement of the large bar due to the estuary narrowing, the “bore reach” also shows a  
512 seaward moving trend. It can be concluded that the morphologically active reach in the Qiantang  
513 Estuary which is strongly influenced by the bore has moved seaward in the last decades.

514

## 515 **6. Conclusions**

516 This study focused on the controls of the inside bar location and dimensions, taking the  
517 Qiantang Estuary as an example. Using idealized model geometries mimicking the planforms of  
518 the Qiantang Estuary in the 1950s and the 2010s, the morphological response of the large bar to  
519 the large-scale coastal embankment project was reproduced first, and then sensitivity analyses of  
520 the convergence length of the estuary and the variations of river discharge were carried out.

521 The morphological response of the large bar to the narrowing project is only several years.  
522 The rapid response is related to the strong tidal currents and large sediment fluxes. With the large-  
523 scale narrowing project of the Qiantang Estuary, the apex of the large inside bar has moved seaward  
524 by 15 km and lowered by 0.86 m. For the first-order estimation of the morphology, the seaward

525 movement can be attributed to the increase of the ratio between river flow and tidal prism at the  
526 mouth. The tidal prism correlates with the estuarine planform under a similar tide. A shorter  
527 convergence length results in a decrease of tidal prism, and an increase of the ratio between river  
528 discharge and tidal prism. The bar movement is also related to the change of tidal asymmetry along  
529 the estuary and subsequently the change of net sediment transport over a tidal cycle.

530 The locations, length and elevations of the inside bar depend on the degree of the convergence  
531 of the estuary. The bar moves seaward, and the bar length decreases with a decrease of the  
532 convergence length. River discharge also plays important role on the bar location and dimensions.  
533 Good relationships exist between river discharge and the location and elevation of the bar apex.  
534 Such relationship would be changed with the change of the estuarine planform.

535 The bar evolution has significant influences on the hydrological regime. The erosion in the  
536 upper reach lowers the local low water level and amplifies the tides, whereas the accumulation in  
537 the downstream slope of the bar increases the local low water level. Particularly, with the change  
538 of the estuarine planform and the seaward movement, the place of the tidal bore occurrence shows  
539 a seaward moving and the strength of the tidal bore shows a decreasing trend, explaining the  
540 historical and recent evolution of the Qiantang bore. In turn, the morphologically active reach in  
541 the estuary strongly influenced by river discharge and the tidal bore also moves seaward.

542

### 543 **Acknowledgments**

544 This research was supported by the National Natural Science Foundation of China (No.  
545 41676085) and Zhejiang Provincial Natural Science Foundation of China (No. LY16D060004).

546 We wish to thank two anonymous reviewers for their constructive comments which improved the  
547 paper greatly.

#### 548 **Data availability**

549 The bathymetric data are available at <https://zenodo.org/record/4915584#.YMC0T5yOM2z>.

550

#### 551 **References**

552 Ahmed, T.S., Egashira, S., Harada, D, and Yorozuya, A., 2019. Sediment transportation and sand  
553 bar deformation owing to tidal currents in Sittaung River Estuary, Myanmar. *Journal of*  
554 *Japan Society of Civil Engineering (Ser. B1)*, 75(2), 1027-1032, doi:  
555 10.2208/jscejhe.75.2\_I\_1027.

556 Bartsch-Winkler, S., and Lynch, D.K., 1988. Catalog of worldwide tidal bore occurrences and  
557 characteristics. *USGS Circular*, 1022, 1-17.

558 Bolla Pittaluga, M., Tambroni, N., Canestrelli, A., Slingerland, R., Lanzoni, S., and Seminara, G.,  
559 2015. Where river and tide meet: The morphodynamic equilibrium of alluvial estuaries.  
560 *Journal of Geophysical Research: Earth Surface*, 120, doi: 10.1002/2014JF003233.

561 Canestrelli, A., Lanzoni, S., and Fagherazzi, S., 2013. One-dimensional numerical modeling of the  
562 long-term morphodynamic evolution of a tidally-dominated estuary: The lower Fly River  
563 (Papua New Guinea). *Sedimentary Geology*, 301, 107-119, doi: 10.1016/j.sedgeo.2013.06.009.

564 Chanson, H., 2012. *Tidal Bores, Aegir, Eagre, Mascaret, Pororoca: Theory and Observations*.  
565 World Science, Singapore.

566 Chanson, H.B., 2011. Two-phase flow in hydraulic jumps at large Froude number. *Journal of*

567           *Hydraulic Engineering*, 137(4), 451-460, doi: 10.1061/(ASCE)HY.1943-7900.0000323.

568   Chen, J.Y., Liu, C.Z., Zhang, C.L., and Walker, H.J., 1990. Geomorphological development and  
569           sedimentation in Qiantang Estuary and Hangzhou Bay. *Journal of Coastal Research*, 6(3),  
570           559-572, doi: 10.2307/4297719.

571   Chen, J.Y., Luo, Z.D., Chen, D.C., Xu, H.G., and Qiao, P.N., 1964. The formation and historical  
572           evolution of the sandbar in Qiantang estuary (in Chinese). *Acta Geographica Sinica*, 30(2),  
573           109-113.

574   Chen, S.M., Han, Z.C., and Hu, G.J., 2006. Impact of human activities on the river reach in the  
575           Qiantang Estuary (in Chinese with English abstract). *Journal of Sediment Research*, (4), 61-  
576           67.

577   Chien, N., Sie, H.S., Chow, C.T., and Lee, Q.P., 1964. The fluvial processes of the big sand bar  
578           inside the Chien Tang Chiang Estuary (in Chinese with English abstract). *Acta Geographica*  
579           *Sinica*, 30(2), 124-142.

580   Choi, K., Kim, D., and Jo, J., 2020. Morphodynamic evolution of the macrotidal Sittaung River  
581           estuary, Myanmar: Tidal versus seasonal controls. *Marine Geology*, 430, 106367, doi:  
582           10.1016/j.margeo.2020.106367.

583   Dai, Z.J., 2021. *Changjiang riverine and estuarine hydro-morphodynamic processes: in the*  
584           *context of Anthropocene era*. Springer.

585   Dai, Z.J., Fagherazzi, S., Mei, X., and Gao, J., 2016. Decline in suspended sediment concentration  
586           delivered by the Changjiang (Yangtze) River into the East China Sea between 1956 and 2013.  
587           *Geomorphology*, 268, 123-132, doi: 10.1016/j.geomorph.2016.06.009.

588 Dai, Z.J., Liu, J.T., Xie, H.L., and Shi, W.Y., 2014. Sedimentation in the outer Hangzhou Bay,  
589 China: the influence of Changjiang sediment load. *Journal of Coastal Research*, 30, 1218-  
590 1225, doi: 10.2112/jcoastres-d-12-00164.1.

591 Dai, Z.J., Mei, X., Darby, S.E., Lou, Y., and Li, W., 2018. Fluvial sediment transfer in the  
592 Changjiang (Yangtze) river-estuary depositional system. *Journal of Hydrology*, 566, 719-  
593 734, doi: 10.1016/j.jhydrol.2018.09.019.

594 Dalrymple, R.W., and Choi, K., 2007. Morphologic and facies trends through the fluvial–marine  
595 transition in tide-dominated depositional systems: a schematic framework for environmental  
596 and sequence-stratigraphic interpretation. *Earth-Science Reviews*, 81(3), 135-174, doi:  
597 10.1016/j.earscirev.2006.10.002.

598 Dam, G., Van der Wegen, M., Labeur, R., and Roelvink, D., 2016. Modeling centuries of estuarine  
599 morphodynamics in the Western Scheldt estuary. *Geophysical Research Letters*, 43 (8), 3839-  
600 3847, doi: 10.1002/2015GL066725.

601 De Ridder, M.P., 2017. *The tidal bore in the Sittaung River - a sensitivity analysis of the*  
602 *propagation*. Unpublished master thesis, The Delft University of Technology.

603 Deltares, 2016. User manual Delft3d-Flow: Simulation of multi-dimensional hydrodynamic flows  
604 and transport phenomena, including sediments.

605 Dijkstra, Y.M., Schuttelaars, H.M., Schramkowski, G.P., and Brouwer, R.L., 2019. Modeling the  
606 transition to high sediment concentrations as a response to channel deepening in the Ems  
607 River Estuary. *Journal of Geophysical Research: Oceans*, 124, 1578-1594, doi:  
608 10.1029/2018JC014367.

609 Dolgoplova, E.N., 2013. The conditions for tidal bore formation and its effect on the transport of  
610 saline water at river mouths. *Water Resources*, 40(1), 16-30, doi:  
611 10.1134/S0097807813010028.

612 Dyer, K.R., 1997. *Estuaries - Physical Introduction*. John Wiley and Sons, Chichester.

613 ECCHE (Editorial Committee for Chinese Harbors and Embayments), 1992. *Chinese Harbours  
614 and Embayments* (Part V, in Chinese). China Ocean Press, Beijing.

615 Fan, D.D., Tu, J.B., Shang, S., and Cai, G.F., 2014. Characteristics of tidal-bore deposits and facies  
616 associations in the Qiantang Estuary, China. *Marine Geology*, 348, 1-14, doi:  
617 10.1016/j.margeo.2013.11.012.

618 Fan, D.D., Tu, J.B., Shang, S., Chen, L.L., and Zhang, Y., 2016. Morphodynamics and sedimentary  
619 facies in a tidal-fluvial transition with tidal bores (the middle Qiantang Estuary, China). In:  
620 Tessier, B., and Reynaud, J.Y., (eds.), *Contribution to Modern and Ancient Tidal  
621 Sedimentology: Proceedings of the Tidalites 2012 Conference*, IAS Special Publication, 48,  
622 75-92.

623 Friedrichs, C.T., and Aubrey, D.G., 1994. Tidal propagation in strongly convergent channels.  
624 *Journal of Geophysical Research*, 99(C2), 3321-3336, doi: 10.1029/93JC03219.

625 Gao, S., and Wang Y.P., 2008. Material fluxes from the Changjiang River and their implications  
626 on the adjoining continental shelf ecosystem. *Continental Shelf Research*, 28, 1490-1500, doi:  
627 10.1016/j.csr.2007.02.010.

628 Geleynse, N., Storms, J.E.A., Walstra, D.J.R., Jagers, H.R.A., Wang, Z.B., and Stive, M.J.F.,  
629 2011. Controls on river delta formation; insights from numerical modelling. *Earth and*

630 *Planetary Science Letters*, 302(1-2), 217-226, doi:10.1016/j.epsl.2010.12.013.

631 Godin, G., 1985. Modification of river tides by the discharge. *Journal of Waterway, Port, Coastal*  
632 *and Ocean Engineering*, 111(2), 257-274, doi: 10.1061/(ASCE)0733-950X(1985)111:2(257).

633 Guo, L.C., Van der Wegen, M., Roelvink, J.A., and He, Q., 2014. The role of river flow and tidal  
634 asymmetry on 1-D estuarine morphodynamics. *Journal of Geophysical Research: Earth*  
635 *Surface*, 119, 2315-2334, doi: 10.1002/2014JF003110.

636 Han, Z.C., Dai, Z.H., and Li, G.B., 2003. *Regulation and Exploitation of Qiantang Estuary* (in  
637 Chinese). China Water Power Press, Beijing.

638 Hibma, A., Stive, M.J.F, and Wang, Z.B., 2004. Estuarine morphodynamics. *Coastal Engineering*,  
639 51, 765-778, doi: 10.1016/j.coastaleng.2004.07.008.

640 Hoitink, A.J.F., Wang, Z.B., Vermeulen, B., Huismans, Y., and Kastner, K., 2017. Tidal controls  
641 on river delta morphology. *Nature Geoscience*, 10, 637-645, doi: 10.1038/ngeo3000.

642 Hoitink, A.J.F., and Jay, D.A., 2016. Tidal river dynamics: implications for deltas. *Reviews of*  
643 *Geophysics*, 54, 240-272, doi: 10.1002/2015RG000507.

644 Hu, P., Han, J.J., Li, W., Sun, Z.L., and He, Z.G., 2018. Numerical investigation of a sandbar  
645 formation and evolution in a tide-dominated estuary using a hydro-sediment-morphodynamic  
646 model. *Coastal Engineering Journal*, 60(4), 466-483, doi: 10.1080/21664250.2018.1529263.

647 Jin, G., Zeng, J., Tang, Z., and Hu, C., 2020. Variation trends of tidal characteristics in the Qiantang  
648 River Estuary and cause analysis (in Chinese with English abstract). *Marine Science Bulletin*,  
649 39(4), 456-463.

650 Lanzoni, S., and Seminara, G., 1998. On tide propagation in convergent estuaries. *Journal of*

651 *Geophysical Research*, 103(C13), 30793-30812, doi: 10.1029/1998JC900015.

652 Leonardi, N., Canestrelli, A., Sun, T., and Fagherazzi, S.E., 2013. Effect of tides on mouth bar  
653 morphology and hydrodynamics. *Journal of Geophysical Research*, 118, 4169-4183, doi:  
654 10.1002/jgrc.20302.

655 Li, G.B., and Dai, Z.H., 1986. Fluvial processes and reclamation of the Qiantang Estuary.  
656 *International Journal of Sediment Research*, 1 (1), 56-66.

657 Lin, B.Y., 2008. *Characteristics of Qiantang Bore* (in Chinese). Chinese Ocean Press, Beijing.

658 Luan, H.L., Ding, P.X., Wang, Z.B., Yang, S.L., and Lu, J.Y., 2018. Morphodynamic impacts of  
659 large-scale engineering projects in the Yangtze River delta. *Coastal Engineering*, 141, 1-11,  
660 doi: 10.1016/j.coastaleng.2018.08.013.

661 Mei, X., Dai, Z., Wei, W., Li, W., Wang, J., and Sheng, H., 2018b. Secular bathymetric variations  
662 of the North Channel in the Changjiang (Yangtze) Estuary, China, 1880-2013: causes and  
663 effects. *Geomorphology*, 303, 30-40, doi: 10.1016/j.geomorph.2017.11.014.

664 Milliman, J.D., Shen, H.T., Yang, Z.S., and Robert, H.M., 1985. Transport and deposited of river  
665 sediment in the Changjiang estuary and adjacent continental shelf. *Continental Shelf Research*,  
666 4, 37-45, doi: 10.1016/0278-4343(85)90020-2.

667 Nienhuis, J.H., Hoitink, A.J.F., and Törnqvist, T.E., 2018. Future change to tide-influenced deltas.  
668 *Geophysical Research Letters*, 45, 3499-3507, doi: 10.1029/2018GL077638.

669 Nnafie, A., Swart, H.E., De Maerschalck, B., Van Oyen, T., Van der Vegt, M., and Van der Wegen,  
670 M., 2019. Closure of secondary basins causes channel deepening in estuaries with moderate  
671 to high friction. *Geophysical Research Letters*, 46(22), 13209-13216, doi:

672 10.1029/2019gl084444.

673 Nnafie, A., Van Oyen, T., De Maerschack, B., Van der Vegt, M., and Van der Wegen, M.,  
674 2018. Estuarine channel evolution in response to closure of secondary basins: an  
675 observational and morphodynamic modeling study of the Western Scheldt Estuary. *Journal of*  
676 *Geophysical Research: Earth Surface*, 123(1), 167-186, doi: 10.1002/2017jf004364.

677 Pan, C.H., and Huang, W.R., 2010. Numerical Modeling of Suspended Sediment Transport  
678 Affected by Tidal Bore in Qiantang Estuary. *Journal of Coastal Research*, 26(6), 1123-1132,  
679 doi: 10.2307/40928851.

680 Pan, C.H., Lu, H.Y., and Zeng, J., 2008. Characteristic and numerical simulation of tidal bore in  
681 Qiantang River (in Chinese with English abstract). *Hydro-Science and Engineering*, (2), 1-9.

682 Partheniades, E.A., 1965. Erosion and deposition of cohesive soils. *Journal of the Hydraulics*  
683 *Division*, 91(HY1), 4204, doi: 10.3109/15622970109026808.

684 Peregrine, D.H., 1966. Calculations of the development of an undular bore. *Journal of Fluid*  
685 *Mechanisms*, 25, 321-330, doi: 10.1017/S0022112066001678.

686 Pye, K., and Blott, S.J., 2014. The geomorphology of UK estuaries: the role of geological controls,  
687 antecedent conditions and human activities. *Estuarine, Coastal and Shelf Science*, 150, 196-  
688 214, doi: 10.1016/j.ecss.2014.05.014.

689 Savenije, H.H.G., 2012. *Salinity and tides in alluvial estuaries* (Second Completely Revised  
690 Edition). <https://salinityandtides.com/>

691 Shimozono, T., Tajima, Y., Akamatsu, S., Matsuba, Y., and Kawasaki, A., 2019. Large-scale  
692 channel migration in the Sittang River Estuary. *Scientific Reports*, 9, 9862, doi: 10.1007/978-

693 981-15-0291-0\_163.

694 Todeschini, I., Toffolon, M., and Tubino, M., 2008. Long-term morphological evolution of funnel-  
695 shape tide-dominated estuaries. *Journal of Geophysical Research*, 113, C05005, doi:  
696 10.1029/2007JC004094.

697 Townend, I., 2012. The estimation of estuary dimensions using a simplified form model and the  
698 exogenous controls. *Earth Surface Processes and Landforms*, 37(15), 1573-1583, doi:  
699 10.1002/esp.3256.

700 Tu, J.B., Fan, D.D., and Voulgaris, G., 2021. Field observations of turbulence, sediment suspension,  
701 and transport under breaking tidal bores. *Marine Geology*, 437(3), 106498, doi:  
702 10.1016/j.margeo.2021.106498.

703 Van der Wegen, M., and Jaffe, B.E., 2014. Processes governing decadal-scale depositional  
704 narrowing of the major tidal channel in San Pablo Bay, California, USA. *Journal of*  
705 *Geophysical Research: Earth Surface*, 119, doi: 10.1002/2013JF002824.

706 Van der Wegen, M., and Roelvink, J., 2008. Long-term morphodynamic evolution of a tidal  
707 embayment using a two-dimensional, process-based model. *Journal of Geophysical Research:*  
708 *Oceans*, 113 (C3), doi: 10.1029/2006JC003983.

709 Van der Wegen, M., and Roelvink, J.A., 2012. Reproduction of estuarine bathymetry by means of  
710 a process-based model: Western Scheldt case study, the Netherlands. *Geomorphology*, 179,  
711 152-167, doi: 10.1016/j.geomorph.2012.08.007.

712 Van Maren, D.S., Winterwerp, J.C., and Vroom, J., 2015. Fine sediment transport into the hyper-  
713 turbid lower Ems River: The role of channel deepening and sediment-induced drag reduction.

714 *Ocean Dynamics*, 65(4), 589-605, doi: 10.1007/s10236-015-0821-2

715 Van Rijn, L.C. (1993), *Principles of sediment transport in rivers, estuaries and coastal seas*, Aqua  
716 Publication, Amsterdam.

717 Wang, Z.B., Jeuken, M., Gerritsen, H., De Vriend, H.J., and Kornman, B., 2002. Morphology and  
718 asymmetry of the vertical tide in the Westerschelde estuary. *Continental Shelf Research*, 22  
719 (17), 2599-2609, doi: 10.1016/S0278-4343(02)00134-6.

720 Wang, Z.B., Louters, T., and De Vriend, H.J., 1995. Morphodynamic modelling of a tidal inlet in  
721 the Wadden Sea. *Marine Geology*, 126, 289-300, doi: 10.1016/S0278-4343(02)-00134-6.

722 Wang, Z.B., Van Maren, D.S., Ding, P.X., Yang, S.L., Van Prooijen, B.C., de Vet, P.L.M.,  
723 Winterwerp, J.C., De Vriend, H.J., Stive, M.J.F., and He, Q., 2015. Human impacts on  
724 morphodynamic thresholds in estuarine systems. *Continental Shelf Research*, 111, 174-183,  
725 doi: 10.1016/j.csr.2015.08.009.

726 Xie, D.F, Gao, S., Wang, Z.B., Pan, C.H, Wu, X., and Wang, Q., 2017b. Morphodynamic modeling  
727 of a large inside sandbar and its dextral morphology in a convergent estuary: Qiantang Estuary,  
728 China. *Journal of Geophysical Research: Earth Surface*, 122(8), 1553-1572, doi:  
729 10.1002/2017JF004293.

730 Xie, D.F., Pan, C.H., Wu, X., Gao, S., and Wang, Z.B., 2017c. Local human activities overwhelm  
731 decreased sediment supply from the Changjiang River: Continued rapid accumulation in the  
732 Hangzhou Bay-Qiantang Estuary system. *Marine Geology*, 392, 66-77, doi:  
733 10.1016/j.margeo.2017.08.013.

734 Xie, D.F., Pan, C.H., Gao, S., and Wang, Z.B., 2018. Morphodynamics of the Qiantang Estuary,

735 China: Controls of river flood events and tidal bores. *Marine Geology*, 406, 27-33, doi:  
736 10.1016/j.margeo.2018.09.003.

737 Xie, D.F., Pan, C.H., Wu, X., Gao, S., and Wang, Z.B., 2017a. The variations of sediment transport  
738 patterns in the outer Changjiang Estuary and Hangzhou Bay over the last 30 years. *Journal of*  
739 *Geophysical Research: Oceans*, 122, 2999-3020, doi: 10.1002/2016JC012264.

740 Xie, D.F., Wang, Z.B., Gao, S., and de Vriend, H.J., 2009. Modeling the tidal channel  
741 morphodynamics in a macro-tidal embayment, Hangzhou Bay, China. *Continental Shelf*  
742 *Research*, 29, 1757-1767, doi: 10.1016/j.csr.2009.03.009.

743 Yang, S.L., Milliman, J.D., Li P., and Xu K.H., 2011. 50,000 dams later: Erosion of the Yangtze  
744 River and its delta. *Global and Planetary Change*, 75, 14-20, doi:  
745 10.1016/j.gloplacha.2010.09.006.

746 Yu, Q., Wang, Y.W., Gao, S., and Flemming, B., 2012. Modeling the formation of a sand bar within  
747 a large funnel-shaped, tide-dominated estuary: Qiantangjiang Estuary, China. *Marine Geology*,  
748 299-302, 63-76, doi:10.1016/j.margeo.2011.12.008.

749 Zeng, J., Chen, G., Pan, C.H., and Zhang, Z.Y., 2017. Effect of dike line adjustment on the tidal  
750 bore in the Qiantang Estuary, China. *Journal of Hydrodynamics*, 29(3), 452-459, doi:  
751 10.1016/S1001-6058(16)60756-4.

752 Zhang, S., Pan, C.H., and Cheng, W.L., 2020. Effect of dike line adjustment on the tidal bore in  
753 the Qiantang Estuary, China (in Chinese with English abstract). *The Coastal Engineering*,  
754 38(1), 130-139.

755 Zhang, W., Ruan, X., Zheng, J., Zhu, Y., and Wu, H., 2010. Long-term change in tidal dynamics

756 and its cause in the Pearl River Delta, China. *Geomorphology*, 120 (3-4), 209-223, doi:  
757 10.1016/j.geomorph.2010.03.031.

758 Zhang, X., Dalrymple, R.W., Yang, S.Y., Lin, C.M., and Wang, P., 2015. Provenance of Holocene  
759 sediments in the outer part of the Paleo-Qiantang River estuary, China. *Marine Geology*, 366,  
760 1-15, doi: 10.1016/j.margeo.2015.04.008. Zhang, X., Lin, C.M., Dalrymple, R.W., Gao, S.,  
761 and Li, Y.L., 2014. Facies architecture and depositional model of a macrotidal incised-valley  
762 succession (Qiantang River estuary, eastern China), and differences from other macrotidal  
763 systems. *Geological Society of America Bulletin*, 126 (3-4), 499-522, doi:  
764 10.1130/B30835.1.

765 Zhang, X.D., Fan, D., Yang, Z., Xu, S., Chi, W., and Wang, H., 2020. Sustained growth of river-  
766 mouth bars in the vulnerable Changjiang Delta. *Journal of Hydrology*, 590, 125450, doi:  
767 10.1016/j.jhydrol.2020.125450.

768 Zhou Z., Coco G., Townend I., et al., 2017. Is “Morphodynamic Equilibrium” an oxymoron. *Earth-*  
769 *Science Reviews*, 165: 257-267, doi: 10.1016/j.earscirev.2016.12.002.

770 Zhou Z., Coco G., Townend I., Gong Z., Wang Z.B., and Zhang C.K., 2018. On the stability  
771 relationships between tidal asymmetry and morphologies of tidal basins and estuaries. *Earth*  
772 *Surface Processes and Landforms*, 43(9): 1943-1959, doi: 10.1002/esp.4366.

773 Zou, Z.N., and Shen, Y.M., 2017. Influence of the reclamation project at Qiantang estuary on the  
774 hydrodynamics and water environment in Hangzhou bay (in Chinese with English abstract).  
775 *Port and Waterway Engineering*, (1), 26-33.

776 **Table and figure captions**

777 **Table 1.** Overview of model input variations in the sensitivity analysis.

778 **Fig.1.** (a) Location of the Qiantang Estuary; (b) Bathymetry of the estuarine reach measured in  
779 November, 2020. The colored shades in panel (a) indicate the progress of the large-scale coastal  
780 embankment project since the 1950s.

781 **Fig. 2.** The laterally averaged longitudinal bathymetries in the 1960s and the 2010s, after [Pan and](#)  
782 [Han \(2017\)](#).

783 **Fig. 3.** Sketch of the modeled estuary. (a) Geometry (top view); (b) initial bathymetry (side view).

784 **Fig. 4.** Modeled bathymetries of the bar at the bar formation (a) and the development of the  
785 longitudinal profiles of the estuary. The arrows across 50 km and 175 km denote the directions  
786 of the cumulative sediment transport over 3 years.

787 **Fig. 5.** Hydrodynamics and sediment transports along the estuary at the initial states. (a) High, low  
788 tidal levels and tidal ranges, (b) the water levels at four instants in the 2010s case, (c) maximum  
789 flood and ebb velocities, (d) the ratio between maximum flood velocity to maximum ebb  
790 velocity, (e) flood and ebb water fluxes over one tidal cycle, (f) the ratio between river flow  
791 and prism, (g) cumulative sediment transport and (h) the net sediment transport over one tidal  
792 cycle.

793 **Fig. 6.** Hydrodynamics along the estuary after 3 years. (a) High, low tidal levels and tidal ranges,  
794 (b) the water levels at four instants in the 2010s case, (c) the maximum flood and ebb velocities,  
795 and (d) the flood and ebb maximum ratio.

796 **Fig. 7.** Longitudinal profiles for various river discharges after 3 years (a) and the bed level changes

797 compared to that of 1000 m<sup>3</sup>/s cases (b).

798 Fig. 8. Simulated correlations between the location (a) and elevation (b) of the bar apex and the  
799 river discharge.

800 **Fig. 9.** Influences of the convergence length on the tidal prism at the estuary mouth (a), and the  
801 river flow - prism ratio along the estuary (b).

802 **Fig. 10.** The cross-sectional averaged longitudinal profiles at the bar formation for the cases of  
803 various estuary convergence.

804 **Fig. 11.** Correlations between the bar dimensions and the convergence length.

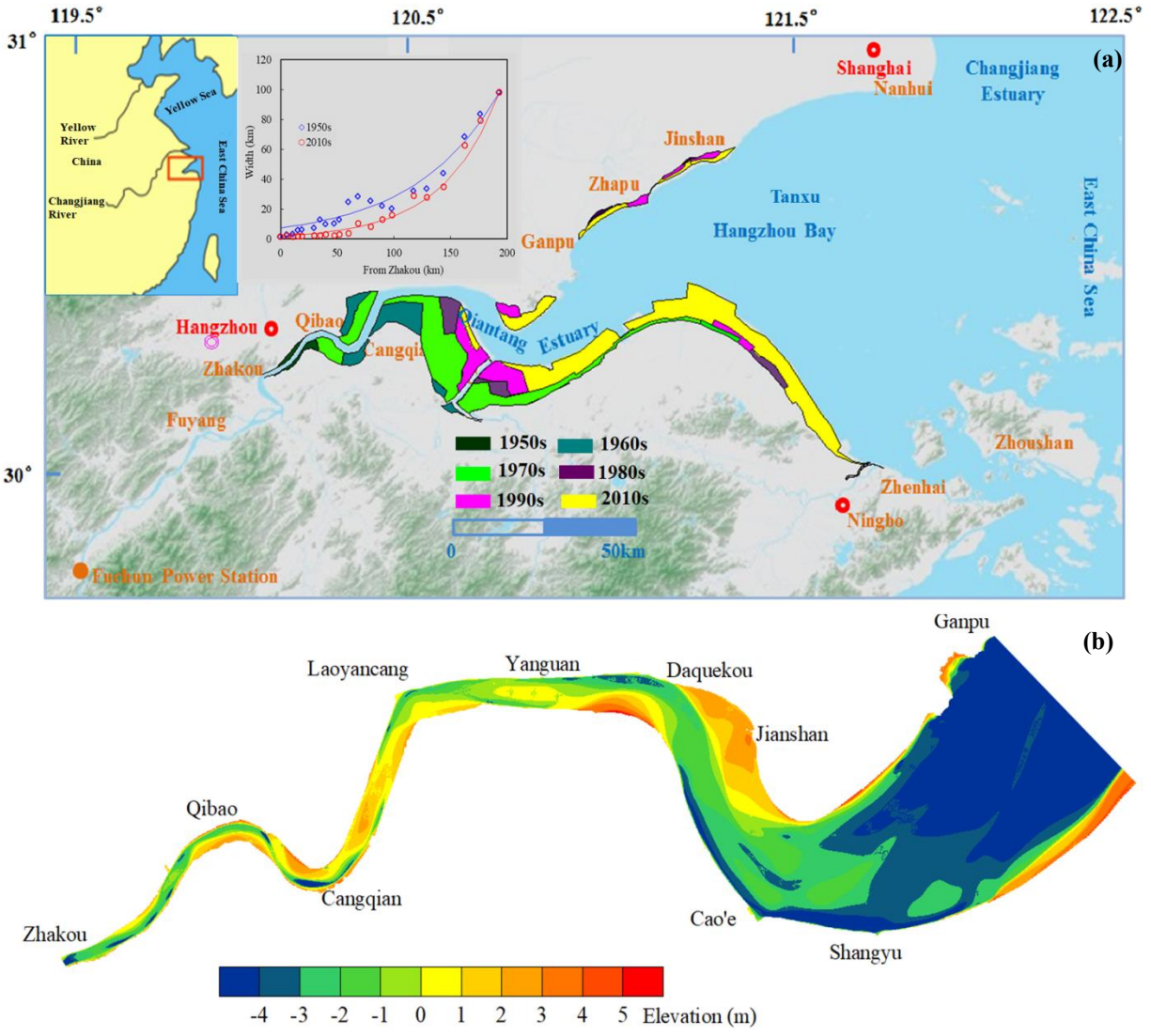
805 **Fig. 12.** Relative Froude number along the estuary after 3 years in the cases of various convergence  
806 lengths.

807

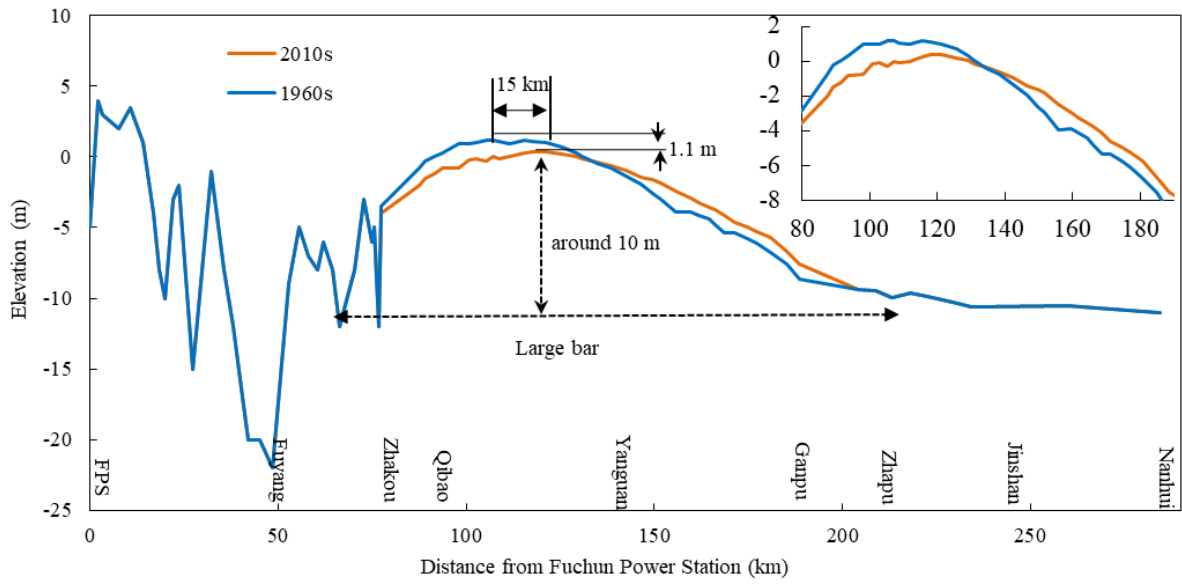
**Table 1.**

Group	Estuary planform	River discharge
1	based on shoreline in the 1950s and 2010s	1000 m <sup>3</sup> /s
2	$L_b=20, 40, 60, 80, 100$ km	1000 m <sup>3</sup> /s
3	based on shoreline in the 1950s	250 - 2000 m <sup>3</sup> /s, with an interval of 250 m <sup>3</sup> /s
4	based on shoreline in the 2010s	250 - 2000 m <sup>3</sup> /s, with an interval of 250 m <sup>3</sup> /s

808

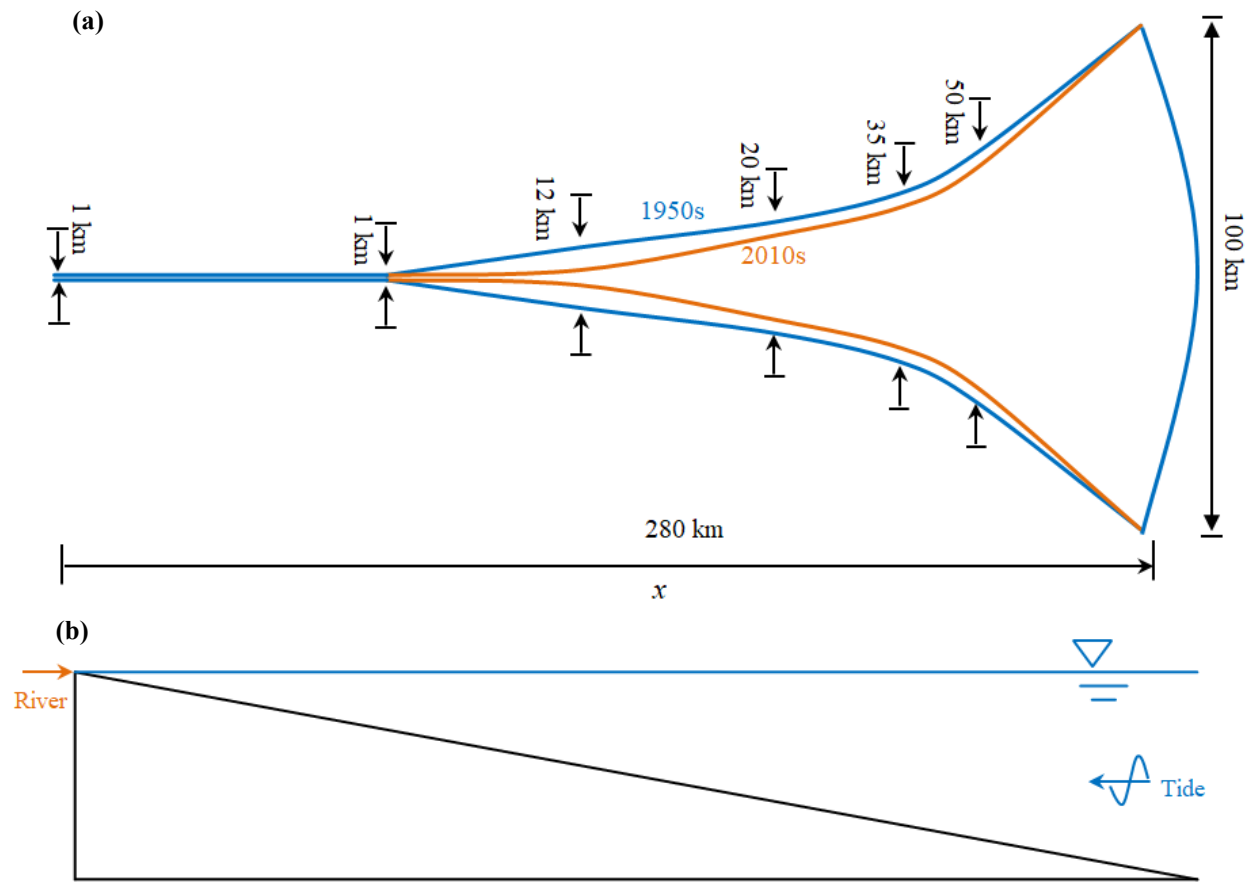


809  
810 **Fig.1.**



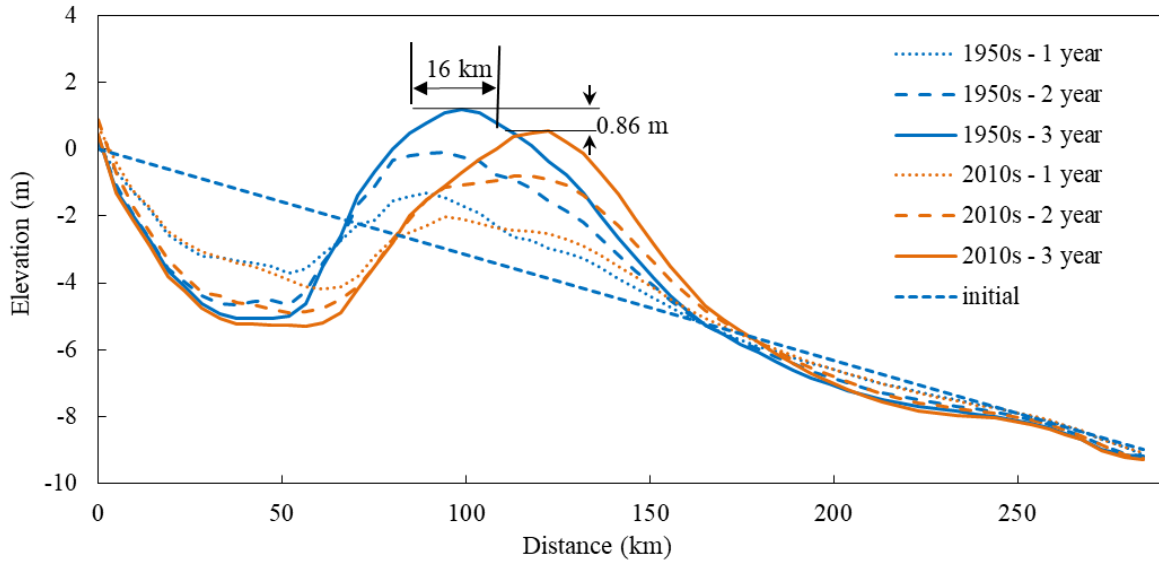
811

812 **Fig. 2.**



813

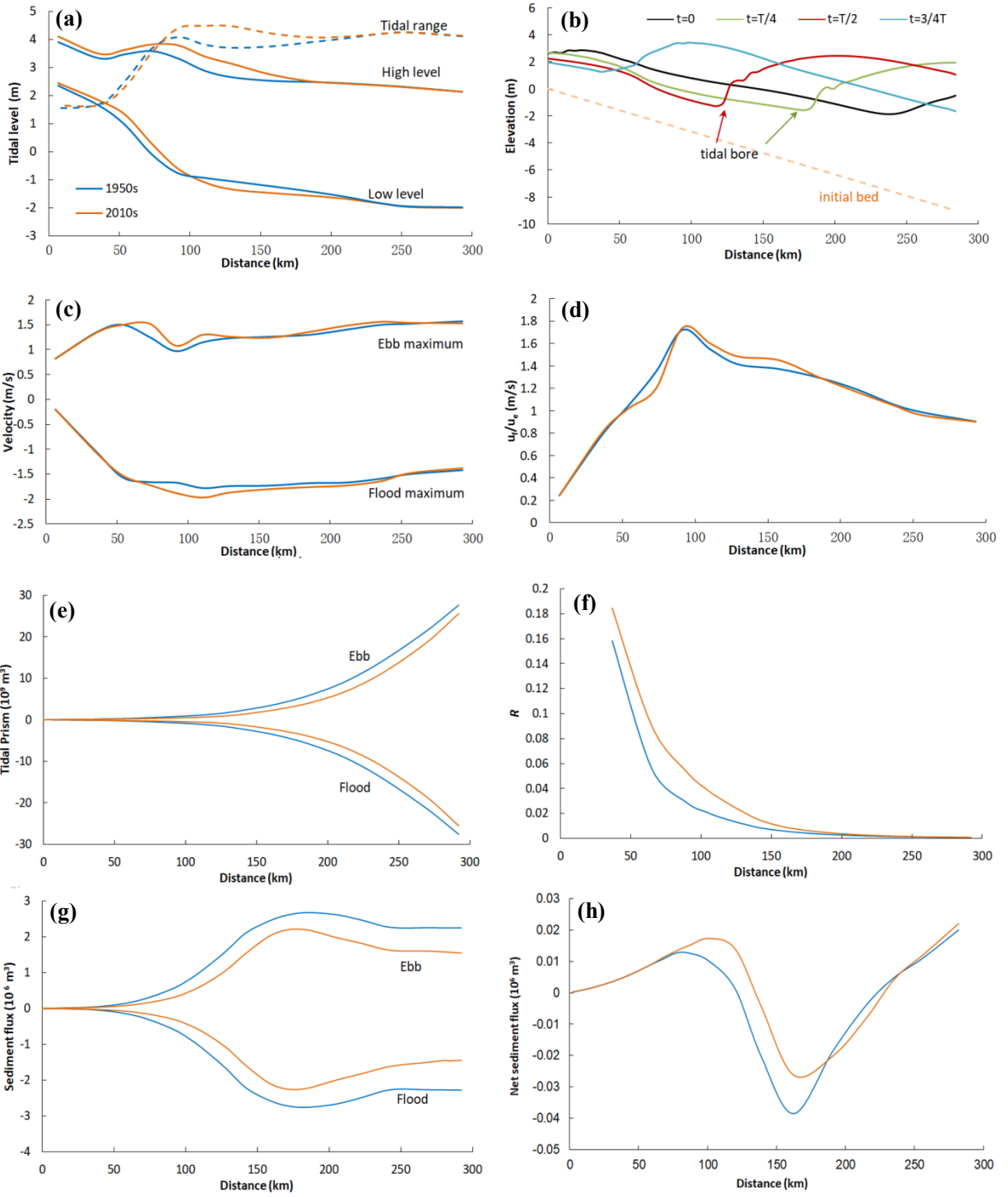
814 **Fig. 3.**



815

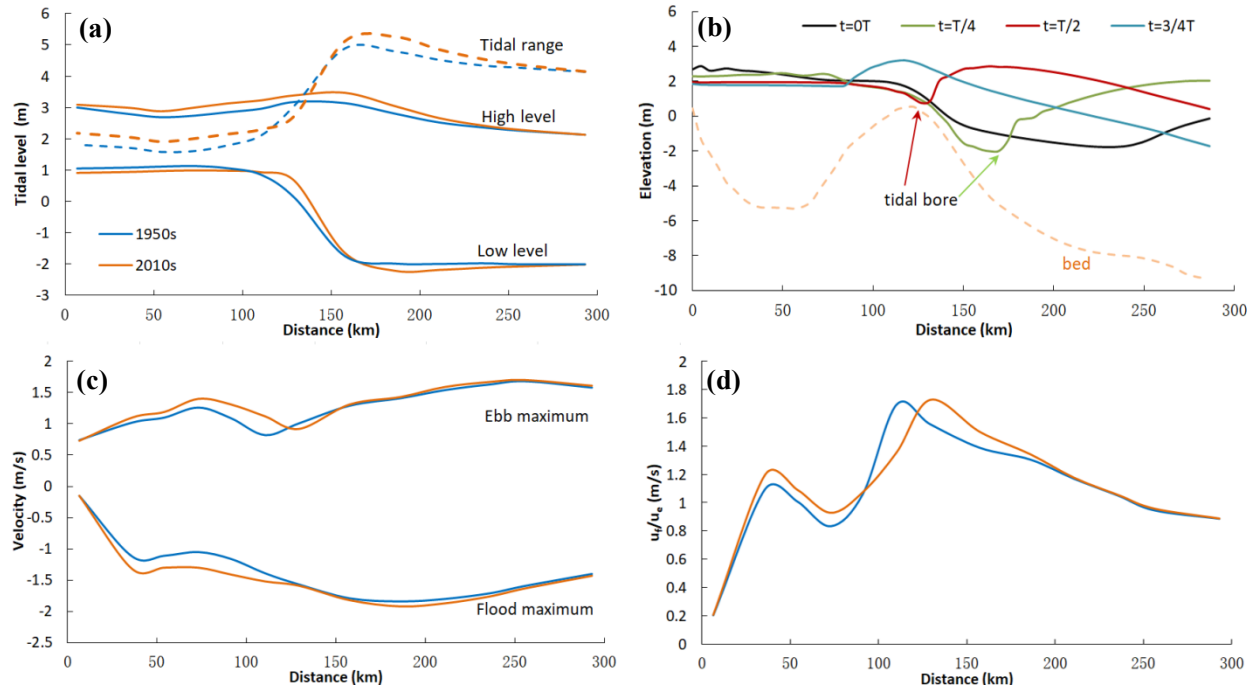
816

**Fig. 4.**



817  
818  
819

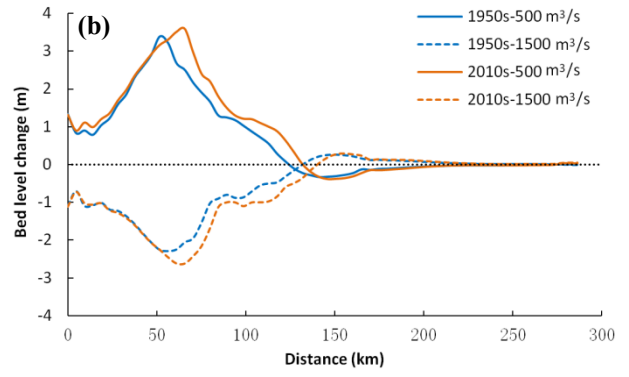
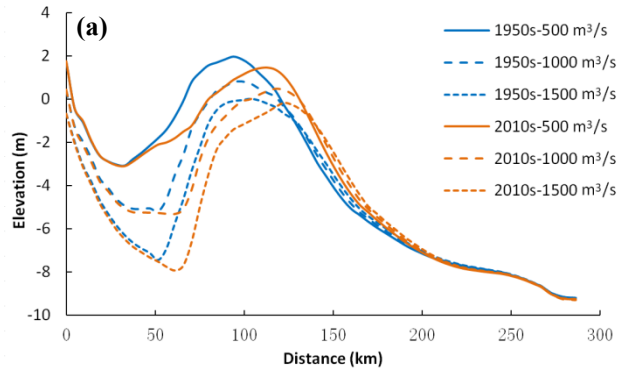
Fig. 5.



820

821

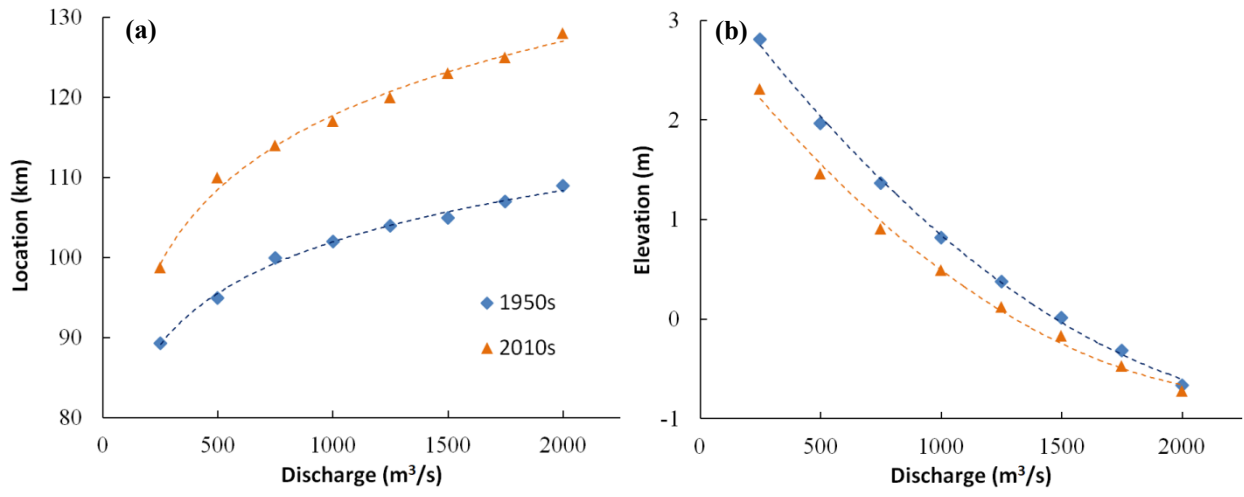
822 **Fig. 6.**



823

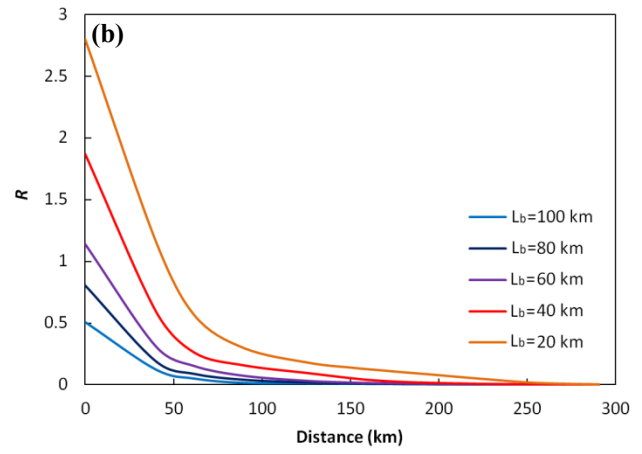
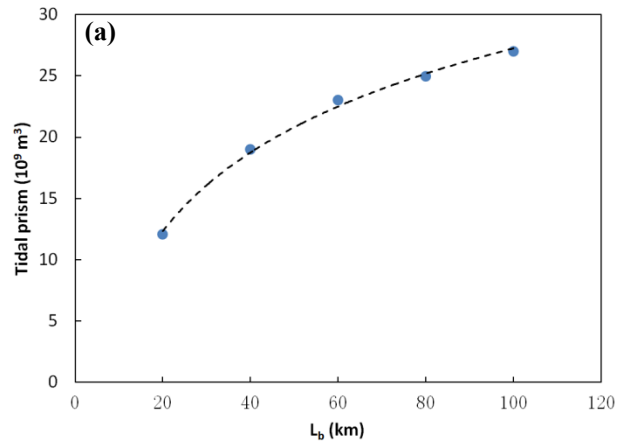
824

**Fig. 7.**

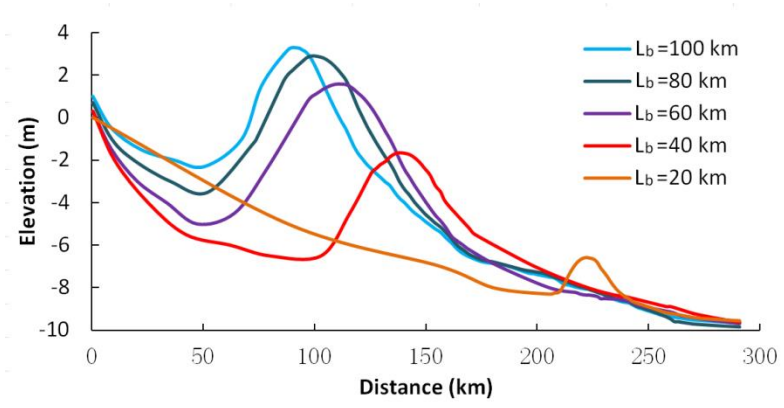


825  
826

**Fig. 8.**

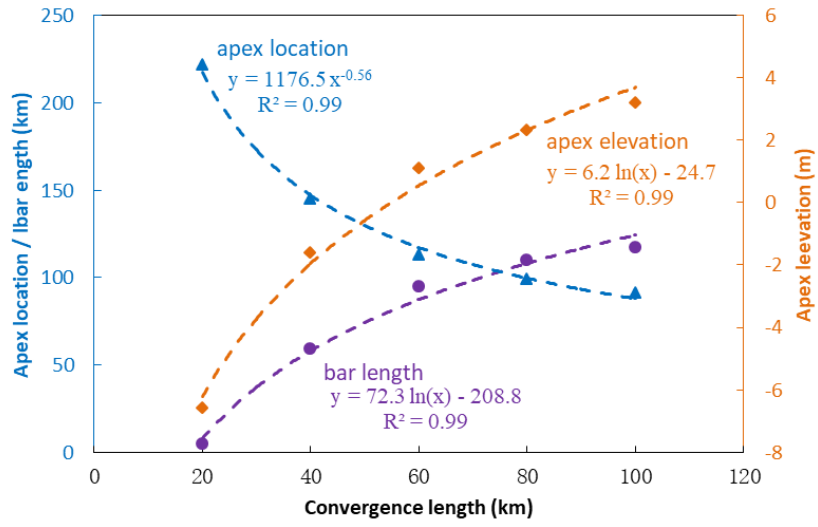


827  
828 **Fig. 9.**

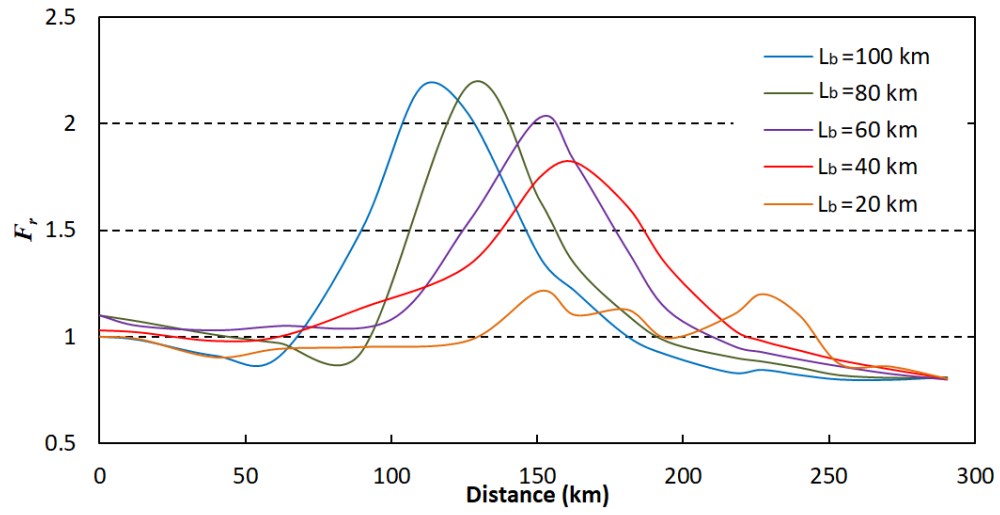


829

830 **Fig. 10.**



831  
 832 **Fig. 11.**



833

834 **Fig. 12.**

835

836

837

838

839

840

841

842

843

844

845

846

847

848

849

850

851